Neuro–degenerative Diseases

Neurodegenerative Dis 2007;4:171–184
DOI: 10.1159/000101842

Peripheral Site Acetylcholinesterase Blockade Induces RACK1-Associated Neuronal Remodeling

Noa Farchi[a, b] Keren Ofek[b] Erez Podoly[b, d] Haiheng Dong[e, f] Yun-Yan Xiang[e, f] Sophia Diamant[b] Oded Livnah[b, d] Jingxin Li[e, f] Binyamin Hochner[a, c] Wei-Yang Lu[e, f] Hermona Soreq[b, c]

Departments of [a]Neurobiology and [b]Biological Chemistry, Institute of Life Sciences and [c]The Israel Interdisciplinary Center for Neuronal Computation, The Hebrew University of Jerusalem, [d]The Wolfson Center for Applied Structural Biology, The Hebrew University of Jerusalem, Jerusalem, Israel; Departments of [e]Anesthesia and [f]Physiology, University of Toronto, Toronto, Ont., Canada

Key Words
Acetylcholinesterase · RACK1 · Neuronal remodeling · BW284C51 · Alternative splicing

Abstract
Background: Peripheral anionic site (PAS) blockade of acetylcholinesterase (AChE) notably affects neuronal activity and cyto-architecture, however, the mechanism(s) involved are incompletely understood. ***Objective:*** We wished to specify the PAS extracellular effects on specific AChE mRNA splice variants, delineate the consequent cellular remodeling events, and explore the inhibitory effects on interchanging RACK1 interactions. ***Methods:*** We exposed rat hippocampal cultured neurons to BW284C51, the peripheral anionic site inhibitor of AChE, and to the non-selective AChE active site inhibitor, physostigmine for studying the neuronal remodeling of AChE mRNA expression and trafficking. ***Results:*** BW284C51 induced overexpression of both AChE splice variants, yet promoted neuritic translocation of the normally rare AChE-R, and retraction of AChE-S mRNA in an antisense-suppressible manner. BW284C51 further caused modest decreases in the expression of the scaffold protein RACK1 (receptor for activated protein kinase βII), followed by drastic neurite retraction of both RACK1 and the AChE homologue neuroligin1, but not the tubulin-associated MAP2 protein. Accompanying BW284C51 effects involved decreases in the Fyn kinase and membrane insertion of the glutamate receptor NR2B variant and impaired glutamatergic activities of treated cells. Intriguingly, molecular modeling suggested that direct, non-catalytic competition with Fyn binding by the RACK1-interacting AChE-R variant may be involved. ***Conclusions:*** Our findings highlight complex neuronal AChE-R/RACK1 interactions and are compatible with the hypothesis that peripheral site AChE inhibitors induce RACK1-mediated neuronal remodeling, promoting suppressed glutamatergic neurotransmission.

N.F. and K.O. contributed equally to this paper.

Introduction

Sustained inhibition of the acetylcholine (ACh) hydrolyzing enzyme AChE is increasingly used to treat patients with Alzheimer's disease [1] or general dementia

KARGER

Fax +41 61 306 12 34
E-Mail karger@karger.ch
www.karger.com

1660–2854/07/0043–0171$23.50/0

Accessible online at:
www.karger.com/ndd

H. Soreq
The Israel Interdisciplinary Center for Neuronal Computation
The Hebrew University of Jerusalem
IL–91904 Jerusalem (Israel)
Tel. +972 2 658 5109, Fax +972 2 652 0258, E-Mail soreq@cc.huji.ac.il

[2]. In addition, several psychoactive drugs inhibit AChE's hydrolytic activity [3], calling for deciphering the biochemical, cellular and molecular reactions to sustained inhibition of neuronal AChE. Importantly, either extracellular and/or intracellular AChE could be inhibited, initiating distinct cellular cascades. Moreover, different anti-AChEs could interact with the enzymatic active site, peripheral anionic site (PAS) or both [4, 5], suggesting differential cellular responses to such blockades. Blocking AChE's active site in the extracellular space should increase the levels and hence the neuro-modulatory activity of ACh [6]. PAS blockade of AChE attenuates such hydrolysis at high substrate concentrations [7] and may trap unbound cationic ligands, interfering with their clearance [8, 9]. In addition, the PAS contributes to neuritogenesis in a manner independent of AChE's hydrolytic activity [10, 11], but which likely involves competition with the AChE-homologous synaptic protein Neuroligin 1 [12, 13]. Therefore, an extracellular PAS blockade, which affects Neuroligin 1 expression, could be predicted to interfere with neuritogenesis and/or modify neuronal cytoarchitecture and synaptic activity. Indeed, our recent study found that inhibition of the peripheral site of AChE induces overexpression of this molecule accompanied by impaired glutamatergic synaptogenesis [14].

At the molecular level, inactivation of AChE's hydrolytic activity induces rapid, yet long-lasting AChE overproduction [15] accompanied by shifted 3′ alternative splicing, replacing the membrane-adhered synaptic AChE-S variant [16] with the soluble, normally rare variant AChE-R and facilitating the neuritic translocation of AChE-R mRNA [17]. When retained intracellularly, AChE-R interaction with the scaffold protein RACK1 recruits PKCβII and enhances the activation of signal transduction events mediated by serine-threonine kinases [18].

RACK1 is notably involved with numerous neuronal properties [19]. In glutamatergic neurons, RACK1 sequentially binds the tyrosine kinase Fyn and the glutamate receptor NR2B, localizing Fyn in close proximity to its NR2B substrate. Once RACK1 is released from its interaction with Fyn, the latter is freed to phosphorylate NR2B, which facilitates NR2B incorporation into the synaptic membrane and prolongs the opening of the NMDA receptor channel [20, 21]. However, the potential effects of these processes on neuronal features remained unexplored.

In-depth evaluation of RACK1's involvement with sustained AChE inhibition should (a) explore the inhibitory effects on interchanging RACK1 interactions; (b) specify the PAS extracellular effects on specific AChE mRNA splice variants, and (c) delineate the consequent cellular remodeling events. With these goals in mind, we treated cultured rat hippocampal neurons with either the AChE active site inhibitor physostigmine, or the extracellular blocker BW284C51 (BW), with both active site and peripheral site blocking activities, or added recombinant AChE-S to the culture medium as a reciprocal control. Follow-up of the cellular reactions to these treatments revealed that PAS, but not active site inhibition caused redistribution of cytoskeletal, signaling and synaptic proteins including RACK1 and suppressed synaptic activities. It also induced selective changes in gene expression and modified AChE mRNA alternative splicing and neuritic translocation events. These findings are compatible with the hypothesis that PAS blockade of neuronal AChE modifies intracellular RACK1 interactions with synaptic protein partners, suppressing glutamatergic neurotransmission.

Materials and Methods

Primary Cell Culture

Dissociated embryonic hippocampal neurons were grown as reported [14]. Neurons were treated at the 3rd or 5th day in culture (DIC), for 3 days with 3–10 μM of the positively-charged PAS ligand, 1,5-bis (4-allyldimethylammoniumphenyl) pentan-3-one dibromide (BW284c51/BW, Sigma, St. Louis, Mo., USA), the active site AChE inhibitor physostigmine or the rat AChE antisense EN101 (12 μg/ml) or inverse oligonucleotide INV101 (12 μg/ml) together with BW [22]. Recombinant human AChE (hAChE, 0.5–3.0 units/ml, Sigma) was added to some cultures at the 4th DIC. To eliminate a possible cholinergic action by the excess AChE, physostigmine (10 μM) was added to the AChE-treated culture dishes at the same time.

Expression of Human Recombinant AChE

Chinese hamster ovary cells (CHO-K1) were grown in Dulbecco's modified Eagle's medium (Biological Industries, Beit Ha'emek, Israel) with 10% fetal calf serum (FCS) and 2 mM L-glutamine at 37°C and 5% CO_2-humidified chamber. Cells were transfected with 6 μg of plasmid DNA encoding either human AChE-S or AChE-R in 75-cm^2 flasks, using Lipofectamine Plus (Gibco BRL Life Technologies, Bethesda, Md., USA) [23]. Transiently transfected cells were harvested 24 h post-transfection, washed with cold phosphate-buffered saline (PBS) and lysed in 0.5% Triton X-100. The supernatant was collected by centrifugation, at 4°C in 14,000 rpm for 30 min, and kept frozen in aliquots at –20°C, until used.

Real-Time RT-PCR

Extracted mRNA from hippocampal cell cultures was subjected to quantitative real-time RT-PCR using a Eurogentec Lithos PCR Hotstar (Eurogentec, Seraing, Belgium) and RNA samples at 100 or 50 nM. Quantification was assessed at the logarithmic

Table 1. Primer pairs and conditions used in RT-RCR

Gene	Primers (annealing, transcription temperatures °C)	
NMDANR1	+ 5′ACCATGTACCGGCACATGG3′ – 5′TGCAGGAGCATTGCTGCGG3′	(67, 90)
RACK1	+ 5′CTCAGCACTACCCCAGCTTC3′ – 5′CTTGCAGTTAGCCAGGTTCA3′	(63, 87)
FYN	+ 5′CTCAGCACTACCCCAGCTTC3′ – 5′CATCTTCTGTCCGTGCTTCA3′	(63, 85)
GAPD	+ 5′TTCACCACCATGGAGAAGGCT3′ – 5′GGCATGGACTGTGGTCATGA3′	(68, 83)
NMDANR2B	+ 5′GTGAGAGCTCCTTTGCCAA3′ – 5′TGAAGCAAGCACTGGTCATC3′	(65, 87)

Primer sequences employed. Shown are the transcripts which were quantified by RT-PCR, the forward and reverse primer sequences and the conditions used in RT-PCR.

phase of the PCR reaction. The PCR annealing and transcription temp. were optimized for each primer pair. The primer pairs and conditions used (Sigma, Jerusalem, Israel) are presented in table 1.

AChE Tests

Cholinesterase (AChE) activity measurements were as detailed elsewhere [24]. For in situ hybridization, hippocampal cultures at the 6th or 8th DIC were fixed by 5.7% paraformaldehyde/4% sucrose in PBS for 30 min, permeabilized in 0.1% Triton X-100 PBS for 20 min and then subjected to fluorescent in situ hybridization as described [25].

Immunocytochemistry

For standard immunohistochemistry, neuronal cultures were fixed in 3.7% paraformaldehyde/4% sucrose in PBS for 30 min, permeabilized in 0.1% Triton X-100 for 15–30 min, blocked in 5% horse serum or 5% BSA for 1 h, and then incubated with primary antibodies for 2 h at room temperature or overnight at 4°C. CY3- or FITC-conjugated secondary antibodies were then added for 1 h. Coverslips were mounted in FluoroMount-G (Electron Microscopy Sciences, Washington, Pa., USA), rinsed thrice with PBS and then mounted for confocal microscopy. Other primary antibodies include: anti-RACK1 (1:2500, Transduction Laboratories, Lexington, Ky., USA), anti-MAP2 (1:400, Chemicon International, Hampshire, UK), anti-Neuroligin 1 (1:300, Synaptic Systems, Göttingen, Germany) and Alexa Fluor 546 phalloidin for staining F-actin (1:400, Molecular Probes Inc, Eugene, Oreg., USA).

Immunoblot Tests

Hippocampal neurons from sister cultures were lysed in ice-cold lysis buffer (50 mM Tris-HCl, 10 mM EDTA, and 1% Triton X-100, pH 8.0) with protease inhibitors. Lysate was cleared by centrifugation, and protein concentrations were assayed by the Bradford method (Bio-Rad, Hercules, Calif., USA). Total proteins were separated on SDS-PAGE (40 μg/lane, unless otherwise indicated) and electroblotted onto a nitrocellulose membrane (Bio-Rad). Membranes were blocked in TBS with Tween 20 (TBST) (10 mM Tris-Cl, 150 mM NaCl, and 0.01% Tween 20, pH 8.0) containing 2% PBS and 3% nonfat dry milk powder (TBSTM) at room temperature for 1 h and then incubated with primary antibodies (overnight at 4°C). Membranes were washed with TBST (three times, 15 min each) and then incubated with appropriate horseradish peroxidase-conjugated secondary antibodies in TBSTM (room temperature, 2 h). After washing, bound antibodies were visualized with an ECL system (Amersham Biosciences, Buckinghamshire, UK). The following commercially available antibodies were used: anti-NR2B (glutamate receptor 2, Chemicon, Calif., USA), anti-FYN (Chemicon), anti-PKCβII and anti-RACK1, all as instructed. Quantitative labeling analysis involved the use of a GS-800 densitometer (Bio-Rad, Tel Aviv, Israel). Specifically, blot films were scanned, and the blot band densities were calculated using the Quantity One program (Bio-Rad). Results were expressed as a percentage of the control band density of a specific protein.

Confocal Microscopy

A Bio-Rad MRC-1024 scan head (Hemel Hempsted, UK), coupled to an inverted Zeiss Axiovert 135M microscope with a ×40 oil immersion objective (N.A. 1.3) was used. Excitation was at 514 nm. Fluorescence emission was measured using a 580df32 bandpass interference filter (580 ± 16 nm) for detecting tetra-methylrhodamine and a 525/40 nm filter for detecting fluorescein. The confocal iris was set to 3 mm. Conditions of scanning took into consideration the overlap of fluorescein fluorescence with the rhodamine filter (as was determined in control experiments). Image processing was with Image Pro Plus 4.5 software (Media Cybernetics, Silver Spring, Md., USA).

Patch-Clamp Recordings

Conventional whole-cell voltage-clamp recordings were made in randomly selected neurons at the 11th DIC at room temperature (22–24°C) using an Axopatch-1D amplifier (Axon Instruments, Foster City, Calif., USA). Patch electrodes (3–4 MΩ) were constructed from thin-walled glass (1.5 mm diameter; World Pre-

cision Instruments, Sarasota, Fla., USA) using a two-stage puller (PP-830, Narishige, East Meadow, N.Y., USA). The standard extracellular solution (ECS) was composed of (in mM) 145 NaCl, 1.3 $CaCl_2$, 5.4 KCl, 25 HEPES, 33 glucose, pH 7.4. To record the NMDA receptor mediated spontaneous excitatory postsynaptic current ($sEPSC_{NMDA}$), glycine (10 μM) together with the selective $GABA_A$ receptor antagonist bicuculline (50 μM) and the non-NMDA glutamate receptor antagonist DNQX (20 μM) were included in the ECS during recordings. The standard intracellular solution (ICS) for recording electrodes consisted of (in mM) 140 CsF, 35 CsOH, 10 EPES, 2 $MgCl_2$, 1 $CaCl_2$, 2 tetraethylammonium, 4 ATP, with final pH at 7.35 and osmolarity at 315 mosm. Specifically, QX314 (100 μM), a Na+-channel blocker, was included in the ICS to eliminate the action potential of the recorded neurons. Following 5–8 min monitoring, the electrical signals (filtered at 2 kHz) were continuously acquired for at least 3 min using the software Clampex (Axon Instruments, Sunnyvale, Calif., USA). The digitized signals of $sEPSC_{NMDA}$ were analyzed with Mini Analysis (Synaptosoft Inc., Decatur, Ga., USA). For analysis of repetitive events of $sEPSC_{NMDA}$, the threshold for detection was set approximately five times higher than the baseline noise. The frequency (number of events/min) and averaged amplitude of $sEPSC_{NMDA}$, as well as the total area (with an arbitrary unit) of $sEPSC_{NMDA}$ valleys within a minute were analyzed.

Molecular Modeling

Homology modeling of human Neuroligin 1 (Q8N2Q7; residues 70–577) and human RACK1 (P63244) was generated by using SWISS-MODEL (URL: http://swissmodel.expasy.org/). Superimposition of the Neuroligin 1 model with the Acetylcholinesterase structure (PDB code 1B41) was done with Swiss Pdb-Viewer (URL: http://www.expasy.org/spdbv/) and PyMol (URL: http://pymol.sourceforge.net/). Complex modeling of RACK1 with the SH2 domain of Fyn (PDB code 1AOT) was generated using the PatchDock server (URL: http://bioinfo3d.cs.tau.ac.il/PatchDock/).

Results

BW Treatment Affects Synaptic NMDA Receptor Functions and Cellular Architecture

In our previous study, we found impaired evoked glutamatergic activity of hippocampal neurons treated with AChE inhibitors (AChE-I). BW, but not physostigmine was found to exert such differences [14]. To further explore the mechanistic differences involved, we recorded spontaneous NMDA receptor mediated excitatory postsynaptic currents ($sEPSC_{NMDA}$) in the 11th DIC neurons. The $sEPSC_{NMDA}$ events were recorded in control neurons (n = 6), which were predictably characterized by repetitive inward current valleys (fig. 1A). BW seriously impaired the synaptic NMDA receptor function, because no $sEPSC_{NMDA}$ was detected in 6 of 11 neurons that were treated with BW. Although $sEPSC_{NMDA}$ events were observed in the remaining 5 BW-treated neurons (fig. 1B), the amplitude (fig. 1C) and frequency (fig. 1D) of $sEPSC_{NMDA}$ valleys were significantly decreased, thus drastically reducing the total area of $sEPSC_{NMDA}$ valleys (fig. 1E). Importantly, these electrophysiological changes were accompanied by conspicuously reduced membrane insertion of GluR2, and to a lesser extent of NR1 subunits [14] (fig. 1F). Together, this outcome demonstrated that the PAS blockade of AChE altered both the cellular organization and synaptic NMDA receptor functions in hippocampal neurons.

Predicting that the BW effects on neuronal spontaneous activity are not limited to synaptic cytoarchitecture alone, BW-treated neurons were further immunolabeled for synaptic and cytoskeletal markers such as the microtubule associated protein-2 (MAP2), the AChE-homologous synaptic protein, Neuroligin 1 and the cytoskeletal protein F-actin (fig. 2A). MAP2 is an important regulator of the initiation of neurite remodeling [26], being highly expressed in neurons before and during neurite outgrowth [27]. MAP2 directly binds to both F-actin and microtubules, presumably coordinating the interaction between neurofilaments [28]. In BW-treated neurons, MAP2 displayed continuous distribution along neuronal processes, demonstrating generally normal neurite extensions with a small but significant 1.3-fold MAP2 increase in treated cells as compared with controls (fig. 2B; n = 11 fields, $p < 0.005$). In contrast, treated cells showed conspicuous reduction in the neuritic labeling of both F-actin and neuroligin 1 (co-labeled in fig. 2B). The neuritic retraction of F-actin, an activator of PKCβII [29] and an important factor for neurite outgrowth [30] was as prominent as that of neuroligin (fig. 2C). However, the somatic densities for neuroligin were increased by 40% in BW-treated neurons ($p < 0.05$), suggesting that it had undergone massive redistribution. The AChE-like synaptic protein neuroligin 1 [31, 32] is involved in synaptic adhesion, inter-neuronal signaling and site-specific recruitment of synaptic proteins during synaptogenesis [33].

BW Inhibition Is Common to Both AChE Variants but Exerts Distinct Effects on AChE-S and AChE-R

The dramatic, yet specific effects of BW at the electrophysiological and cytoarchitectural levels raised the quest for the intracellular consequences of AChE inhibition. To study the differences between the active and the anionic site AChE inhibitors (fig. 3A) we determined their inhibition potency for the recombinant 3′ splice variants AChE-S and AChE-R (fig. 3C). The extracellular peripheral site inhibitor BW or the membrane permeable, catalytic site inhibitor physostigmine were added to extracts of CHO-

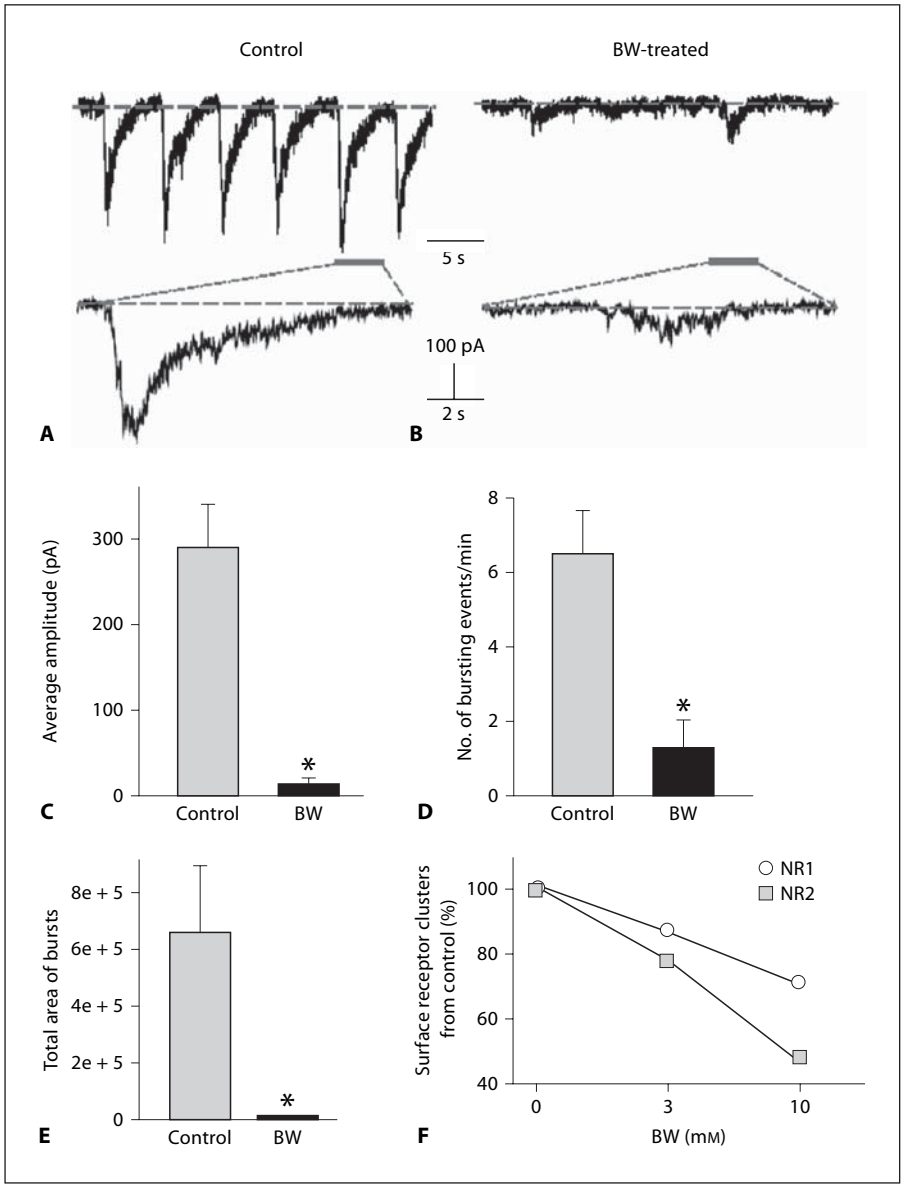

Fig. 1. BW treatment impairs excitatory synaptic transmission. Illustrated are representative traces of $sEPSC_{NMDA}$ in naive (**A**) and BW-treated neurons (**B**). The single $sEPSC_{NMDA}$ valleys that are extended with a shorter time-scale are shown below. In comparison to naive cells, BW-treated neurons display significant reductions in the peak amplitude (**C**, control: 288 ± 49 pA, n = 6; BW: 16.2 ± 8 pA, n = 5; $p < 0.001$), frequency (**D**, control: 6.4 ± 1.2 events/min; BW: 1.3 ± 0.7 events/min; n = 5; $p < 0.005$) and total area (**E**, arbitrary unit, control: 6.4 ± 1.3, n = 6; BW: 0.17 ± 0.09, n = 5; $p < 0.005$) of $sEPSC_{NMDA}$ valleys. (**F**) Surface clusters of NR1 and NR2B subunits of glutamate receptors are reduced in BW-treated neurons. * 0.005.

K1 Chinese hamster ovary cells that were genetically engineered to over-express AChE-S or AChE-R. BW and physostigmine inhibited the two AChE variants to nearly identical extents, with IC_{50} values of 32 and 70 nM, respectively (fig. 3D). This was compatible with previously reported values for human AChE [34]. Nevertheless, when added to cultured primary rat hippocampal neurons, these two inhibitors exerted distinct cellular effects [14].

The employed cholinesterase inhibitors encompass different regions in the AChE molecule (fig. 3A), and are both known to effectively block the hydrolytic activity of AChE [35]; NCBI PP22303). This raised the question whether neuroligin 1 (NCBI Q8N2Q7), which shows 32% identity (206/638 residues) and 46% similarity (299/638 residues) with 13% gaps (89 residues) to AChE [36] could also interact with PAS inhibitors. To examine this query, we constructed a model of neuroligin 1 based on its sequence homology to α/β-hydrolase fold enzymes (fig. 3B). Our model showed that AChE's PAS predictably consists of aromatic and anionic residues, whereas the equivalent residues in neuroligin 1 are of aliphatic and polar nature. The dissimilarity between PAS regions of these two proteins suggested low propensity for binding of BW to neuroligin 1.

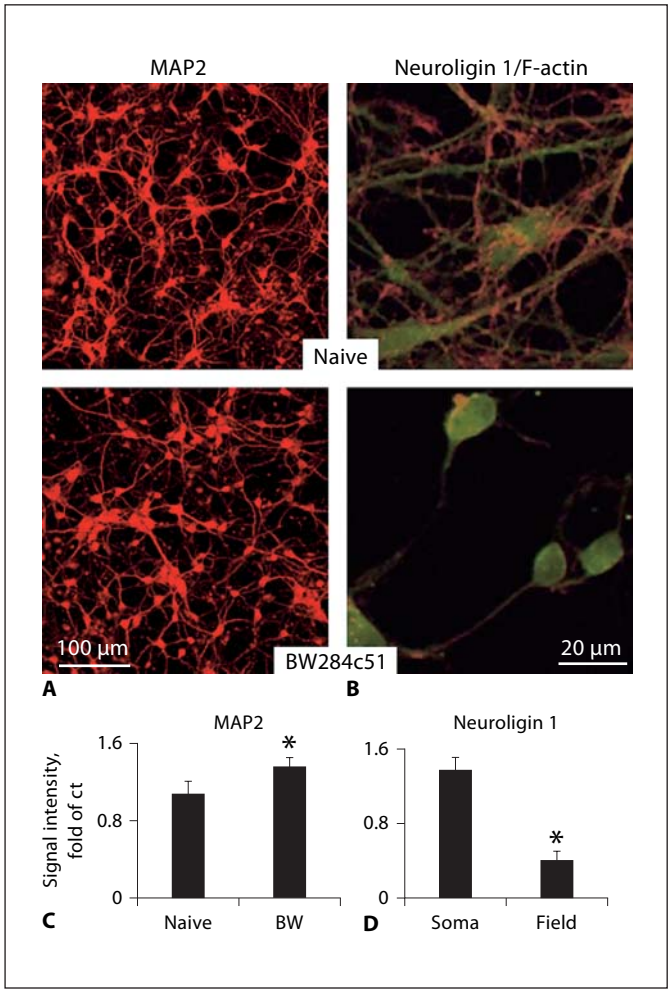

2

Fig. 2. Selective changes in the cellular translocation of synaptic and cytoskeletal proteins. **A** The microtubule associated protein MAP2 increases in level yet maintains unmodified distribution. Shown are representative micrographs from immunocytochemistry staining for MAP2 in naive and BW284c51 cultures. Note increased levels under BW284c51 (* $p < 0.005$). **B** F-actin (green) and Neuroligin 1 (red) double labeling. **C**, **D** Quantification of MAP2 and Neuroligin 1 labeling in somatic areas and total fields of BW-treated cells. Note elevated cell body labeling (reflecting mid-plane data) for MAP2 and reduced field covering all focal planes for Neurologin 1.

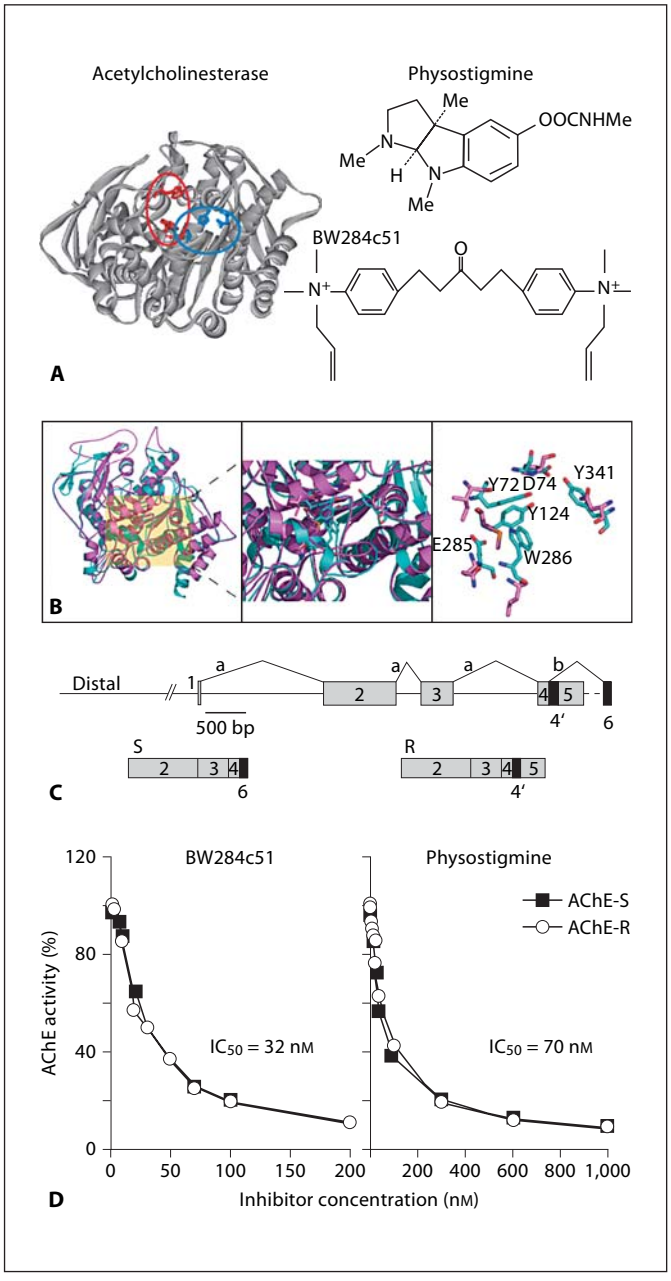

3

Fig. 3. Recombinant AChE-S and-R display similar sensitivities to peripheral and active site inhibitors. **A** Shown is the crystal structure of AChE (PDB ID code 1C2B) with active and peripheral sites, highlighted in blue and red, respectively, and the structures of two corresponding blockers presented (physostigmine for the active site, BW284c51 for the PAS). **B** Left: Superimposition of a Neuroligin 1 model (magenta) and the AChE structure (cyan) reveals structural homology. Middle: Focusing on the PAS region of AChE and the equivalent location in Neuroligin 1 demonstrates dissimilarity of side chain characteristics between the two proteins. Right: AChE's PAS residues – Y72, D74, Y124, E285, W286 and Y341 (cyan) include anionic and aromatic side chains, in contrast to the Neuroligin 1 residues organized structurally in the same location that include side chains of aliphatic and polar character. **C** Alternative splicing of the *ACHE* gene (top) yields AChE-S mRNA (S) and AChE-R mRNA (R). Distal promoter(s) (Distal) are noted by an extended line [17]. Linkage of exons 2, 3, and 4 is common to both variants (option a). The R transcript includes at its 39 terminus pseudointron 4 and exon 5; option b yields the S transcript by connecting exon 4 to 6. **D** Inhibition curves for recombinant human AChE-R or AChE-S proteins from transfected CHO-K1 cells in the presence of increasing concentrations of BW284c51 and physostigmine. Note the closely similar effects of both inhibitors on the two AChE variants and closely similar inhibition potency.

PAS Inhibition Alters AChE Gene Expression

Fluorescent in situ hybridization (FISH) using selective probes against AChE-R (intron 4′) and AChE-S mRNA (exon 6; fig. 4A) showed that close to 60% of the BW-treated cells over-expressed both AChE-S and ChE-R mRNA transcripts in comparison with controls, in agreement with previous findings [16]. Confocal microscopy quantification of the labeling density in the somatic area of BW-treated neuronal populations showed 1.6- and 1.4-fold increases in AChE-R and AChE-S mRNAs, respectively (fig. 4B; n = 120 cells, 5 cultures each, $p < 0.03$, Student's t test). To test if the effect is due to catalytic inhibition of the AChE enzyme, we added 10 μM physostigmine to the primary neurons. In spite of its similar potency to inhibit AChE's hydrolytic activity of both variants, physostigmine had no effect on either of these variant AChE transcripts, unlike hippocampal slices which reacted to physostigmine by inducing AChE overexpression [37]. That the cultured neurons were refractory to the administration of muscarinic agents [14] may explain this difference. We then added EN101, an antisense oligonucleotide targeted at exon 2 of AChE mRNA which selectively suppresses AChE-R mRNA [18]. At the concentration of 1.99 μM, EN101 attenuated the BW-induced accumulation of both AChE transcripts, with a predictably more effective reduction in AChE-R than in AChE-S mRNA (fig. 4C; n = 40 cells, 4 cultures each, $p < 0.05$). INV101, an inversely oriented oligonucleotide of similar nucleotide composition to EN101 showed no significant effect on AChE mRNA levels of BW-treated neurons, demonstrating sequence specificity for EN101. Importantly, reciprocal application for three days of exogenous purified recombinant AChE-S induced a feedback downregulation of both AChE mRNA transcripts (fig. 4C). Thus, suppressed AChE-R production but not inhibited catalytic activity could abrogate the BW effect, compatible with the hypothesis that it reflected noncatalytic features particular to the AChE-R splice variant.

Distinct Neuritic Redistributions of AChE mRNA Splice Variants under BW Blockade

Next, we wished to analyze the BW effect on the neuritic distribution of AChE-S and AChE-R mRNAs, knowing that PAS blockade by BW drastically reduces neurite growth of cultured hippocampal neurons [14]. To evaluate the neuritic translocation profiles of AChE mRNA transcripts, we quantified the corresponding FISH signals at nuclear foci, somatic and neuritic regions, respectively (fig. 5A). Nuclear export was analyzed by comparing the labeling patterns of AChE-S and -R mRNAs in nuclear

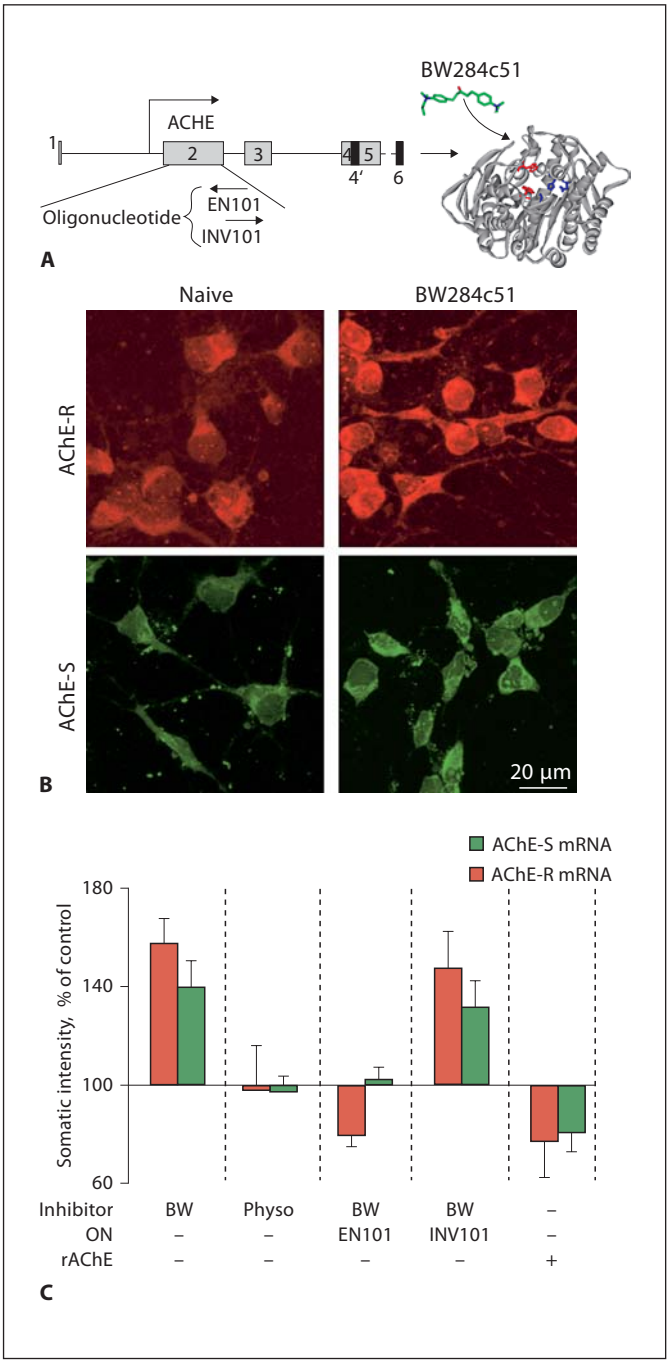

Fig. 4. Differential changes in AChE-S and AChE-R mRNA levels in treated neurons. **A** Schematic presentation of ACHE gene and its protein. Note that the EN101 antisense sequence is complementary to 20 nucleotides within exon 2 and INV101 is inverse to the EN101 sequence. **B** AChE-R (red) or AChE-S (green) mRNA were labeled by in-situ hybridization in hippocampal cultures with or without (naive) BW284c51 (10 μM, 3 days in culture). Note the increased labeling intensities in treated cells. **C** Averaged results for somatic labeling densities at the noted treatments. Results are presented as % increase of naive sister cultures of each experiment.

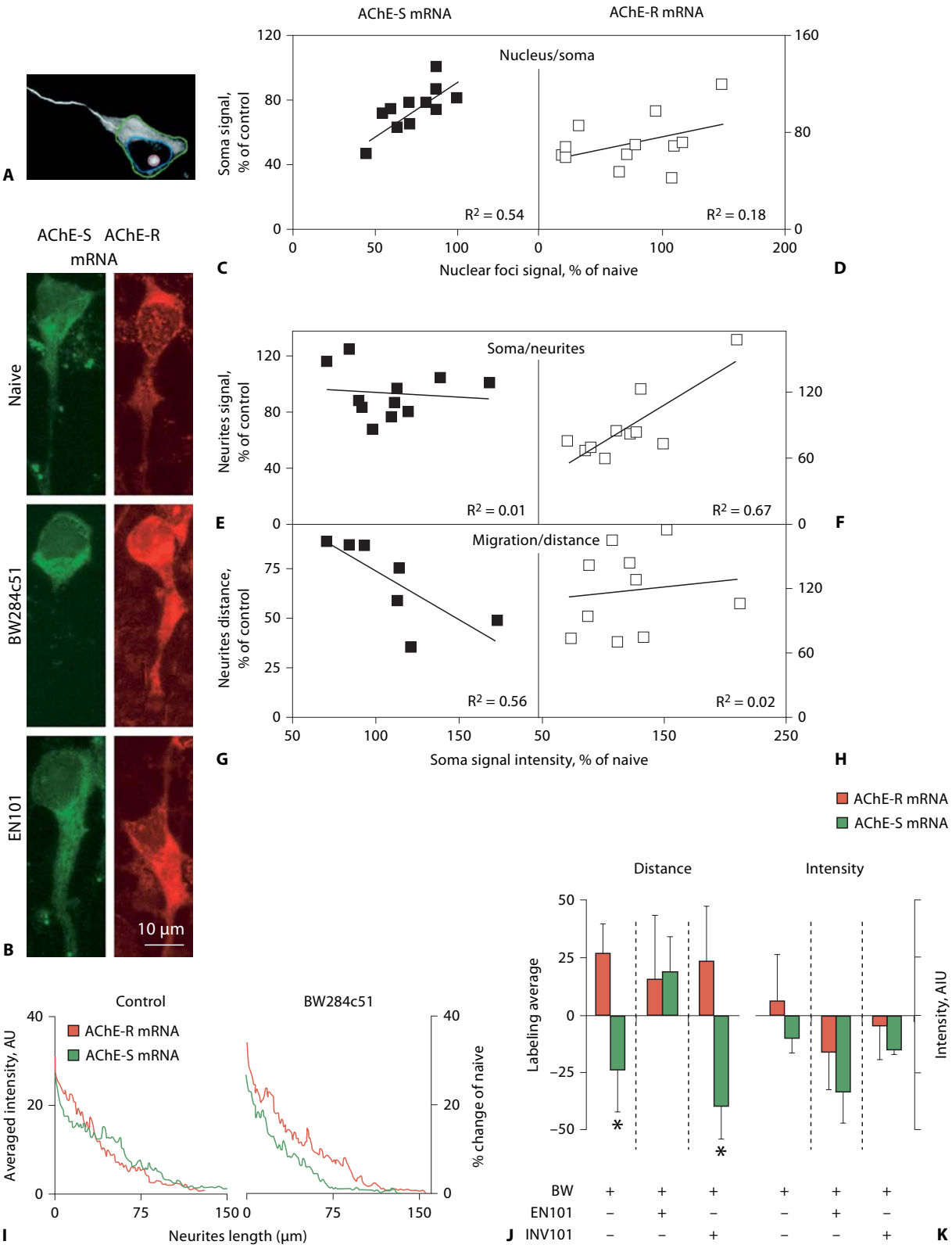
A
AChE-S mRNA
AChE-R mRNA
Nucleus/soma
Soma signal, % of control
R² = 0.54
R² = 0.18
Nuclear foci signal, % of naive
C
D
AChE-S mRNA
AChE-R mRNA
Naive
BW284c51
EN101
10 µm
B
Soma/neurites
Neurites signal, % of control
R² = 0.01
R² = 0.67
E
F
Migration/distance
Neurites distance, % of control
R² = 0.56
R² = 0.02
Soma signal intensity, % of naive
G
H
AChE-R mRNA
AChE-S mRNA
Distance
Intensity
Labeling average
Intensity, AIU
BW
EN101
INV101
J
K
Control
BW284c51
Averaged intensity, AU
% change of naive
Neurites length (µm)
I

foci and soma. Representative cells with BW-induced increases, or EN101-induced decreases in somatic AChE-S mRNA are shown in figure 5B, demonstrating the neuritic translocation of AChE mRNA transcripts. Data from differently treated cultures were collectively analyzed for the relationship between mRNA levels at the nucleus and soma under a relatively wide range of optical densities (n = 304 cells from 12 cultures). A significant positive correlation ($R^2 = 0.54$, $p < 0.01$, F test) emerged between nuclear to somatic AChE-S mRNA levels (fig. 5C). AChE-R mRNA displayed less pronounced correlation between these two parameters (fig. 5D; $R^2 = 0.18$, $p < 0.16$), indicating different efficiencies of nuclear export for these two AChE transcripts. However, neuritic AChE mRNA densities demonstrated a direct correlation with the somatic density for the AChE-R, but not the AChE-S variant (fig. 5E and F, $R^2 = 0.01$; $R^2 = 0.67$, $p < 0.003$). Inversely, the neurite and soma densities of AChE-S showed a negative correlation, i.e. the higher the AChE-S mRNA levels in the soma, the shorter was its translocation distance in neurites, indicating decreased translocation of the S-variant from the soma to neurites (fig. 5G; $R^2 = 0.56$, $p < 0.05$). Reciprocally, the decreased AChE-S levels were accompanied by intensive AChE-R labeling at distant neurites, independent of the somatic levels of AChE-R mRNA (fig. 5H; $R^2 = 0.02$, $p < 0.7$), and highlighting the differential regulation of transport of these two transcripts.

To evaluate the specific spatial organization of AChE mRNA transcripts in BW-treated neurons, both the labeling intensity and the distance from the somatic border at the midline axis of the main neuronal process were measured. A comparative analysis of both the -R and -S mRNAs in control cultures revealed declining labeling intensities with distance along the neuronal process (fig. 5B, I). Importantly, BW-treated neurons in sister cultures displayed a significant decrease in the neurite density of AChE-S mRNA, accompanied by facilitated AChE-R mRNA intensity. In addition, quantitative analysis revealed that in BW-treated neurons, the AChE-S mRNA labeling distance was 27% shorter (fig. 5J; $p < 0.01$) whereas the AChE-R mRNA labeling distance was 21% longer, than that in control neurons (fig. 5I, J; 4 cultures of each, treated: 70 cells; control: 65 cells, $p < 0.05$). Significantly, in cells that were co-treated with BW and EN101, the S-transcript labeling distance within neurites increased considerably, compatible with the inverse soma-to-neurites relations of AChE-S mRNA (fig. 5J). EN101 did not exert significant effects on AChE-R labeling distances in neurites of BW and EN101-treated cells, compatible with the weak association between the somatic levels of AChE-R and its translocation distance (fig. 5J). In addition, BW-treated neurons exhibited modestly increased average density of AChE-R mRNA (fig. 5K), suggesting that the BW treatment mostly affects mRNA transport. Since these results were normalized to those of control cultures, the inverse nature of the observed effects should reflect genuine differences. Having extended our previous findings [16], the present results indicated that PAS blockade induced AChE-S mRNA retraction back to the cell bodies, while facilitating AChE-R mRNA translocation to the neurites.

Fig. 5. BW treatment yields neuritic AChE-R dominance and retraction of AChE-S. **A** Sample cell, demonstrating analyzed cellular regions: somatic border is indicated by a green line. The nucleus is marked by a blue line, within which a nuclear focus of labeling is marked with pink contour. A white line indicates the Neurite midline. **B** Example neurons showing the varied distributions of labeled AChE-R (red) or AChE-S (green) mRNA within the above cellular regions in different treated cultures. Note that BW284c51 suppresses, whereas EN101 increases AChE-S mRNA in the neurites, with reciprocal pattern of AChE-R mRNA labeling. **C**, **D** Labeled mRNA signals at the somatic area were plotted as a function of the labeling in nuclear foci and for AChE-S (**C**) and AChE-R (**D**). Note that the nucleus to soma transport of AChE-S is pronouncedly more affected by its nuclear concentration than AChE-R. **E**, **F** Labeled mRNA signals in Neurites (total signal at the midline axis of the main neurite) were plotted as a function of the somatic labeling density, for AChE-S (**E**) and AChE-R (**F**). Note that only AChE-R mRNA translocation from the soma to neurite demonstrates direct correlation. **G**, **H** Translocation efficacy from soma to neurite was also analyzed by plotting the distance traveled by each mRNA within the neurite as a function of somatic labeling density (**G**, **H**) for AChE-S (**G**) or AChE-R (**H**). Note that AChE-S mRNA translocation distance decreases with increasing somatic signal. **I** Averaged from 40 cells in a single culture, labeling intensities of AChE-R and mRNA are shown as a function of the distance along the neurite in naive and BW284c51 treated neurons. **J** Averaged results for mRNA labeling distance along the midline axis in neuronal processes under BW284c51, BW284c51 with EN101 (12 μg/ml) or INV101 (12 μg/ml). Note that the decreased transport of AChE-S mRNA under BW284c51 is rescueable under EN101, suggesting that it depends on nascent transcripts production. **K** Same as **B** but for labeling intensity. Note that EN101 tends to reduce the neurites labeling density of both transcripts, although insignificantly so.

Co-Altered Expression of RACK1, Synaptic and Cytoskeletal Gene Products under Blockade of AChE's PAS

Because BW treatment modified the distribution of AChE-R mRNA, we suspected that this treatment altered the co-localization of its corresponding protein partners, and consequently modified cellular signaling events [38,

39]. To test this hypothesis, we co-labeled AChE-R mRNA and the RACK1 protein. Greenish-yellow labeling indicated co-localization of neuronal AChE-R mRNA and the RACK1 protein (fig. 6A). BW treatment decreased RACK1 immunolabeling in the soma. However, reduction was yet more prominent in the neurites (fig. 6B, left; n = 36 cells, $p < 0.05$). To further examine potential changes in the neuritic distribution pattern of RACK1, we performed quantitative population analyses of the somatic middle section in individual cells. In naive cells, the distribution of RACK1 across a width section through the soma which was normalized by extrapolation, displayed a U-shaped profile with a 2nd degree polynomial fit, representing higher protein density along the circumference submembrane (fig. 6B, right; n = 32 cells of each). In contrast, BW-treated neurons demonstrated homogenous cytosolic distribution, indicating a significant modification of RACK1 positioning.

RACK1 plays a role in intracellular signaling [18, 38]. Therefore, we first tested whether blockade of AChE altered its expression and affected additional synaptic and cytoskeletal mRNAs. Real time RT-PCR analysis of RNA preparations from three different treated and untreated cell cultures, all normalized to the housekeeping glyceraldehyde 3-phosphate dehydrogenase (GAPDH) mRNA, showed marked and reproducible decreases in the mRNAs for RACK1, the tyrosine kinase Fyn and the NR2B but not the NR1 subunit of the NMDA receptor (between measurements SEM = 0.06; fig. 6C). Corresponding changes were observed in protein blot analyses of two different treated and untreated hippocampal cell cultures. Thus RACK1, FYN and NR2B, but not PKCβII showed marked decreases in BW-treated cells (fig. 6C, inset).

In BW-treated neurons, the reduced RACK1 and Fyn protein products, particularly in the sub-membrane circumference could predictably alter intracellular signaling [19], especially by modifying RACK1-Fyn interactions. Thus, RACK1 binds Fyn and NR2B [21] or PKCβII and AChE-R [38]. The PKC-RACK1 heterodimer could possibly act as a core for further interactions of RACK1, for example with tyrosine kinases (Src/Fyn, fig. 6D–F). Mo-

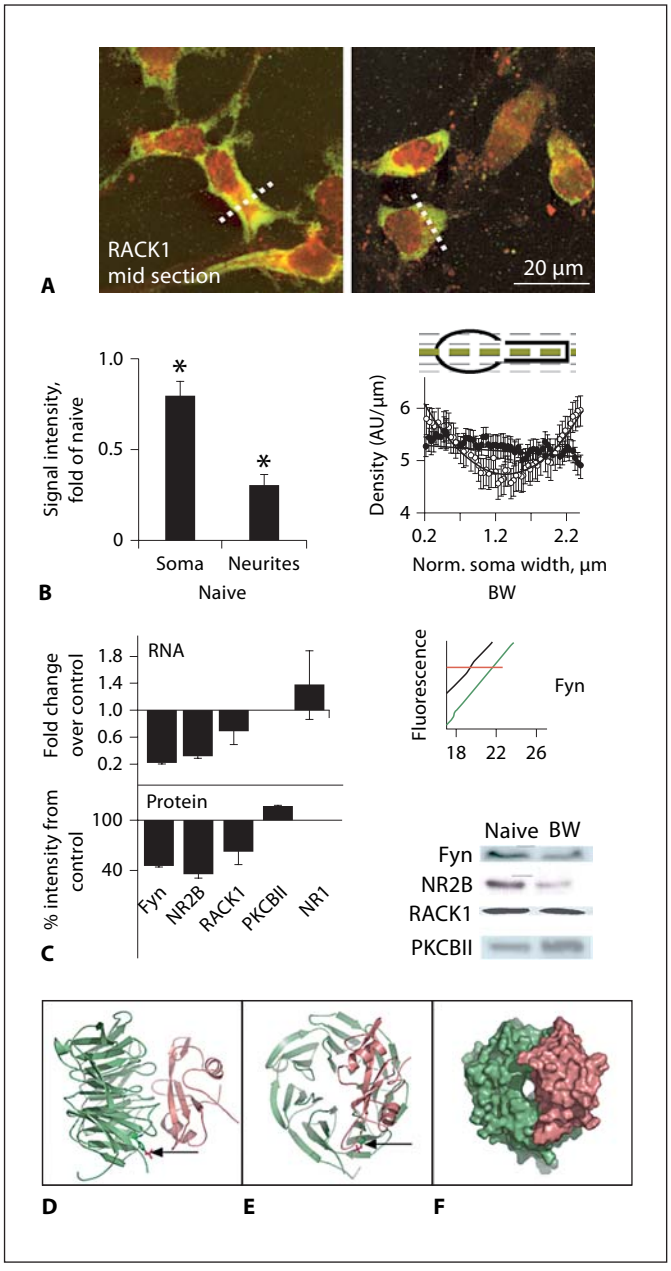

Fig. 6. Selective changes in expression levels and cellular translocation. **A** Double labeling of AChE-R mRNA (red) and RACK1 protein (green) in naive and BW-treated cells. **B** Left: Averaged quantification of RACK1 signals in soma and process areas, normalized (norm.) to naive cells. Right: Analysis of a cross width section through the soma of RACK1 labeled cells (see example of dotted white line in **A**) in naive and BW284c51-treated cultures. **C** BW-induced changes in the mRNA and protein levels of synaptic and cytoskeletal elements were quantified by real-time RT-PCR and protein immunoblots (left columns). Insets show RT-PCR kinetics and representative immunoblot samples for naive and BW-treated cells. Data is presented as fold change of the values measured in BW-treated compared to untreated cells. **D** Predicted model of RACK1 and the SH2 domain of Fyn suggests its interaction next to phosphotyrosine 246 (arrow) that is located in blade six of RACK1. **E** A 90° rotation along a vertical axis clockwise relative to **D**. **F** Surface representation of the orientation displayed in **E**.

lecular modeling suggested that when PKC occupies one face of RACK1's blade six, Fyn may interact with its opposite side, which contains tyrosine (Y) 246 (the essential phosphorylation site for RACK1-Src binding [40]. Reciprocal considerations extend to the ternary complex RACK1-PKC-AChE-R: AChE-R may interact with the same face of blade six in RACK1 as Fyn [19, 38], suggesting that Fyn and AChE-R compete on RACK1 binding. Src activity (and perhaps the homologous Fyn) is necessary for phosphorylating RACK1's Y228/Y246 and for the subsequent binding of RACK1 to the SH2 domain of Src (or Fyn), which follows PKC activation [41]. This, in turn, could explain how AChE-R accumulation under BW could interfere with RACK1/Fyn interaction, impairing NR2B phosphorylation and attenuating synaptic activity.

Discussion

Our previous study shows that PAS blockade of AChE decreases neurite growth, and reduces the number of dendritic spines and synapses, as well as the surface expression of glutamate receptors, demonstrating an inhibition of the formation of glutamatergic synapses. In our current study, we observed that PAS blockade significantly increases the total amount of pre- and postsynaptic proteins, including neuroligin and NR1. Together, these studies suggest that PAS blockade suppresses synaptogenesis by interrupting the molecular organization of synapses, with consequent somatic accumulation of synaptic proteins within neurons. The mechanism(s) underlying these feedback responses to PAS blockade of AChE molecules in primary hippocampal neurons were found to include RACK1 dislocation from the submembrane circumference, suppressed Fyn expression, reduced NR2B membrane insertion and impaired spontaneous sEPSCs accompanied by up-regulation and neuritic translocation of AChE-R mRNA. Our findings thus support the hypothesis that anti-AChEs change both neuronal cyto-architecture and physiological functions through modulating RACK1-mediated interactions with different protein partners.

PAS Blockade of Extracellular AChE Induces Intracellular Translocation of AChE Isoforms

BW induces subcellular rearrangement of AChE mRNA variants (reduction of AChE-S mRNA and accumulation of AChE-R mRNA in neurites), consequent modifications in neuritic protein transport and suppressed synaptic function. Interruption of synaptic function is one of the earliest features of Alzheimer's disease [42]. Our findings raise the possibility that modified AChE gene expression is causally involved.

Translocation of specific mRNAs to subcellular compartments of neurons has been suggested as a regulatory mechanism, by which specific protein isoforms can be synthesized in their functioning site during synaptogenesis [43] or plasticity responses [44, 45]. AChE's regulation of neurite growth [10, 46] has been attributed to extracellular intervention with AChE's adhesion features [47]. These features largely depend on the PAS properties, compatible with our findings that BW treatment modified the neuritic trafficking of alternative AChE mRNA transcripts and induced massive translocation of key proteins. To this end, the mechanism(s) by which PAS blockade induces this chain of intracellular events is not yet clear.

AChE-R, unlike AChE-S mRNA displayed direct correlation between its somatic to neuritic densities. AChE mRNA labeling at nuclear foci has been characterized as responsive to antisense treatment [16, 48], supporting the notion that AChE mRNA transcripts are subject to dynamic recycling in these sites.

PAS Blockade-Induced Modifications Interrupt Postsynaptic and Cytoskeletal Protein Targeting

PAS blockade by BW impaired excitatory synaptic transmission and glutamate receptor functions. BW is a blocker of the nicotinic AChR as well [11]. Nevertheless, we have previously shown that atropine and mecamylamine, specific inhibitors of nicotinic and muscarinic receptors correspondingly, do not impair the glutamate currents [14]. This reinforces our hypothesis that the BW effects we observed act through its AChE inhibition feature and do not reflect its nicotinic receptor interaction. On the other hand, most excitatory synapses are found on the distal dendritic spines. Translocation of more AChE-R mRNAs to the dendritic compartment may represent a high expression level of AChE-R molecules in dendritic spines, consequently altering the molecular organization of synapses. More specifically, increase in the AChE-R isoform could alter synaptic protein targeting intracellularly by competitively binding to RACK1 and consequently interrupting RACK1-mediated targeting of synaptic proteins (such as NR1). PAS blockade by BW decreased neuronal, and in particular neuritic RACK1 concentrations, possibly due to both reduced production and active retraction, while increasing the translocation of AChE-R transcripts. RACK1 further retracted from the sub-membrane compartment. While AChE-R mRNA and RACK1 likely use independent trafficking mecha-

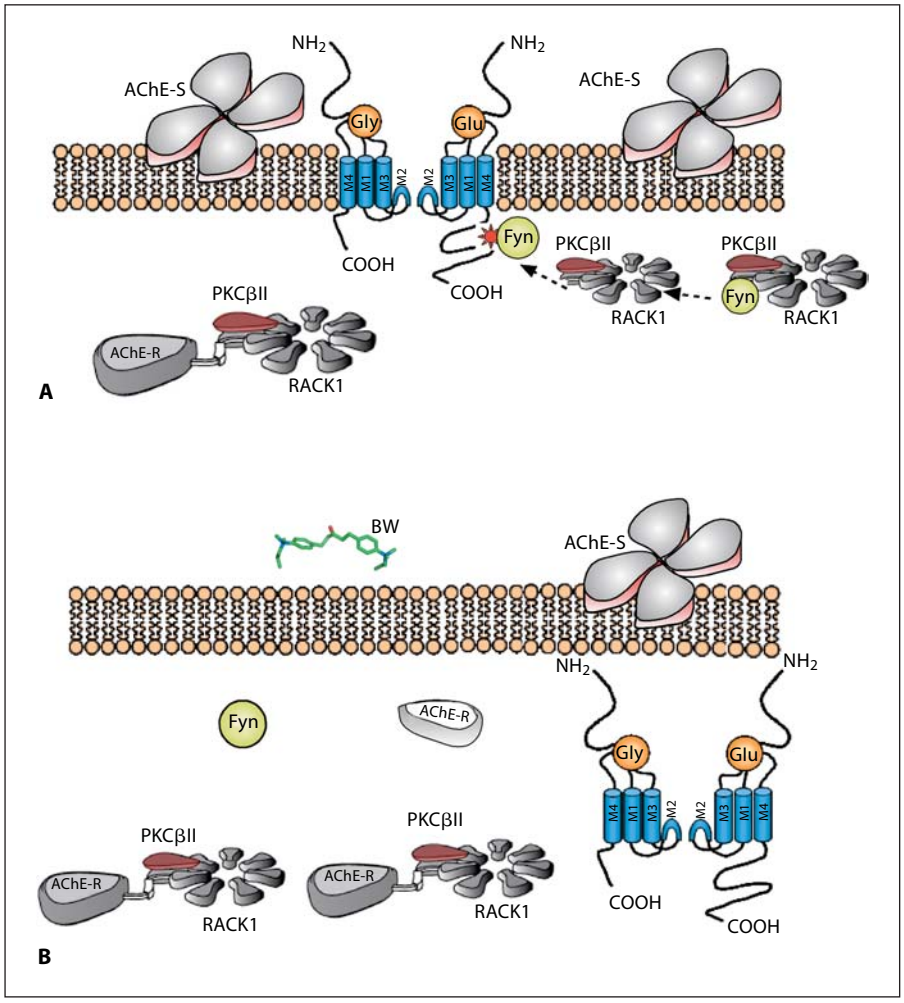

Fig. 7. Suggested mechanism. Shown is a schematic model of the analysed proteins under naive and the BW exposure conditions. **A** In naive cholinoceptive neurons, AChE-S tetramers adhere to the synaptic membrane and the cytoplasm includes scarce AChE-R molecules. RACK1 is free to interact with Fyn and facilitate its phosphorylation. Consequent release of phosporylated Fyn leads to NR2B chains phosphorylation and insertion into the plasma membrane, where they create active ion channels. **B** BW exposure increases AChE-R and decreases RACK1 levels in the vicinity of the synaptic membrane. This supports the substitution of RACK1-Fyn complexes with AChE-R-RACK1-PKCβII complexes, interferes with NR2B phosphorylation by Fyn and impairs NR2B insertion into the membrane, suppressing NMDA channel activities.

nisms, replacement of neuritic AChE-S with AChE-R and the modified somatic RACK1 concentrations may increase the formation of AChE-R/RACK1 complexes. The drastic alteration of neuritic RACK1 targeting under PAS blockade of AChE appears to involve triple RACK1 complexes with AChE-R and PKCβII [38]. This may possibly interfere with RACK1 interaction with Fyn and its transport to the NMDA receptor [19].

BW-Mediated AChE-R-RACK1-PKCβII Accumulation May Compete with RACK-1 Fyn-NR2B Interactions

In the brain, NMDA receptors are found both in the cytoplasm of neurons as well as at excitatory synapses [49] and are assembled from two subunits, NR1 and NR2 which may be phosphorylated in serine and tyrosine residues, reciprocally [50]. Importantly, trafficking of NMDA receptors to the synaptosomal fraction is mediated via a tyrosine kinase-dependent mechanism [51]. Fyn is a Src-homologous tyrosine kinase which phosphorylates, among other targets, the NR2B subunit of NMDA receptors. Fyn kinase-null mice are indeed deficient in certain forms of long-term potentiation [52]. Our findings, and the molecular modeling work, are both compatible with the suggestion of BW-induced downregulation of FYN-RACK1-NR2B complexes. Retraction of RACK1 from neurites and the plasma cell membrane was followed by a decrease in NR2B tyrosine phosphorylation, causing mal-trafficking of NMDA receptors to the synaptic membrane, and impairing synaptic activity. PKC interactions may therefore be a necessary preceding step to Fyn binding, which induces a conformational change in RACK1 that exposes an otherwise inaccessible tyrosine in Fyn for phosphorylation. The altered RACK1 positioning at submembrane compartments, in conjunction with its down-regulation would jointly impair PKC/RACK1 interactions, attenuating Fyn phosphorylation

and preventing the transport of Fyn to the NMDA receptor. The increased potential to produce AChE-R in neurites further predicts increased competition by AChE-R on RACK1/Fyn interactions. Figure 7 presents this concept graphically.

Neuronal mRNAs are translocated to specific subcellular compartments via kinesin or dynein motors along actin microfilaments [53]. BW treatment altered the neuritic targeting of the cytoskeletal protein MAP2, an important regulator of neurite growth patterns [26]. MAP2 includes three microtubule-binding repeats [54] that stabilize and confer rigidity to the microtubules [55]. Under certain conditions, for example following the activation of protein kinase A (PKA), MAP2 also associates with the actin cytoskeleton, suggesting that its actin-related functions are regulated by phosphorylation [56]. Homodimerized MAP2 molecules bound to microtubules crosslink them to actin filaments [28]. The significant downregulation of F-actin under BW exposure, the phosphorylation-dependent nature of MAP2-actin interactions and the upregulation of MAP2 under PAS blockade of AChE might hence indicate modified stability and rigidity of the microtubules.

The altered trafficking of synaptic and skeletal proteins in cultured neurons raises the possibility that relevant situations may occur in vivo, e.g. during brain development [46], under stress or exposure to organophosphates [15, 16, 57], or under chronic treatment with anti-AChE reagents, for example in Alzheimer's disease patients [58]. Cholinergic activation notably facilitates long-term potentiation [59, 60] and protects neurons by upregulating NMDA receptor function [61, 62]. The physiological relevance of these processes is evident from the corresponding changes in behavior and memory [18, 38]. That antisense interference with AChE gene expression (e.g. [18]) suppresses the corresponding phenotypes indicates a causal role of AChE overproduction in these events. RACK1 responses to extracellular PAS AChE inhibitors can thus reveal functional cascades with considerable relevance to higher brain functions.

Acknowledgements

We thank Drs. Naomi Melamed-Book (Jerusalem) and German Sumbre (Berkeley) for assistance. This research was supported by the Israel Science Fund (618y02), the European Union (the APOPIS LSHM-CT-2003-503330 Project and the Network of Excellence-LSH-2004-1.1.5-3), the German-Israeli Project (DIP-G-3.2) and the Israeli Ministry of Science 618/02-1 to (H.S.); and by the Canadian Institutes of Health Research (to W.-Y. L.).

References

1 Cummings JL: Alzheimer's disease. N Engl J Med 2004;351:56–67.
2 Parnetti L: Therapeutic options in dementia. J Neurol 2000;247:163–168.
3 Burt T: Donepezil and related cholinesterase inhibitors as mood and behavioral controlling agents. Curr Psychiatry Rep 2000;2: 473–478.
4 Silman I, Sussman JL: Acetylcholinesterase: 'classical' and 'non-classical' functions and pharmacology. Curr Opin Pharmacol 2005; 5:293–302.
5 Soreq H, Seidman S: Acetylcholinesterase: new roles for an old actor. Nat Rev Neurosci 2001;2:294–302.
6 Gu Q: Neuromodulatory transmitter systems in the cortex and their role in cortical plasticity. Neuroscience 2002;111:815–835.
7 Szegletes T, Mallender WD, Thomas PJ, Rosenberry TL: Substrate binding to the peripheral site of acetylcholinesterase initiates enzymatic catalysis. Substrate inhibition arises as a secondary effect. Biochemistry 1999;38:122–133.
8 Bourne Y, Taylor P, Radic Z, Marchot P: Structural insights into ligand interactions at the acetylcholinesterase peripheral anionic site. EMBO J 2003;22:1–12.
9 Van Belle D, De Maria L, Iurcu G, Wodak SJ: Pathways of ligand clearance in acetylcholinesterase by multiple copy sampling. J Mol Biol 2000;298:705–726.
10 Day T, Greenfield SA: A non-cholinergic, trophic action of acetylcholinesterase on hippocampal neurones in vitro: molecular mechanisms. Neuroscience 2002;111:649–656.
11 Olivera S, Rodriguez-Ithurralde D, Henley JM: Acetylcholinesterase promotes neurite elongation, synapse formation, and surface expression of AMPA receptors in hippocampal neurones. Mol Cell Neurosci 2003;23: 96–106.
12 Grifman M, Galyam N, Seidman S, Soreq H: Functional redundancy of acetylcholinesterase and neuroligin in mammalian neuritogenesis. Proc Natl Acad Sci USA 1998;95: 13935–13940.
13 Scheiffele P: Cell-cell signaling during synapse formation in the CNS. Annu Rev Neurosci 2003;26:485–508.
14 Dong H, Xiang YY, Farchi N, Ju W, Wu Y, Chen L, Wang Y, Hochner B, Yang B, Soreq H, Lu WY: Excessive expression of acetylcholinesterase impairs glutamatergic synaptogenesis in hippocampal neurons. J Neurosci 2004;24:8950–8960.
15 Kaufer D, Friedman A, Seidman S, Soreq H: Acute stress facilitates long-lasting changes in cholinergic gene expression. Nature 1998; 393:373–377.
16 Meshorer E, Erb C, Gazit R, Pavlovsky L, Kaufer D, Friedman A, Glick D, Ben-Arie N, Soreq H: Alternative splicing and neuritic mRNA translocation under long-term neuronal hypersensitivity. Science 2002;295: 508–512.
17 Meshorer E, Soreq H: Alternative AChE splice variants in stress-related neuropathologies. Trends Neurosci 2006;29:216–224.
18 Nijholt I, Farchi N, Kye M, Sklan EH, Shoham S, Verbeure B, Owen D, Hochner B, Spiess J, Soreq H, Blank T: Stress-induced alternative splicing of acetylcholinesterase results in enhanced fear memory and long-term potentiation. Mol Psychiatry 2004;9: 174–183.
19 Sklan EH, Podoly E, Soreq H: RACK1 has the Nerve to act: structure meets neurofunction. Prog Neurobiol 2006;78:117–134.
20 Lu WY, Xiong ZG, Lei S, Orser BA, Dudek E, Browning MD, MacDonald JF: G-protein-coupled receptors act via protein kinase C and Src to regulate NMDA receptors. Nat Neurosci 1999;2:331–338.

21 Yaka R, He DY, Phamluong K, Ron D: Pituitary adenylate cyclase-activating polypeptide (PACAP(1–38)) enhances N-methyl-D-aspartatereceptorfunctionandbrain-derived neurotrophic factor expression via RACK1. J Biol Chem 2003;278:9630–9638.
22 Brenner T, Hamra-Amitay Y, Evron T, Boneva N, Seidman S, Soreq H: The role of readthrough acetylcholinesterase in the pathophysiology of myasthenia gravis. Faseb J 2003;17:214–222.
23 Perry C, Sklan EH, Birikh K, Shapira M, Trejo L, Eldor A, Soreq H: Complex regulation of acetylcholinesterase gene expression in human brain tumors. Oncogene 2002;21: 8428–8441.
24 Bryk B, BenMoyal-Segal L, Podoly E, Livnah O, Eisenkraft A, Luria S, Cohen A, Yehezkelli Y, Hourvitz A, Soreq H: Inherited and acquired interactions between ACHE and PON1 polymorphisms modulate plasma acetylcholinesterase and paraoxonase activities. J Neurochem 2005;92:1216–1227.
25 Meshorer E, Toiber D, Zurel D, Sahly I, Dori A, Cagnano E, Schreiber L, Grisaru D, Tronche F, Soreq H: Combinatorial complexity of 5′ alternative acetylcholinesterase transcripts and protein products. J Biol Chem 2004;279:29740–29751.
26 Gonzalez-Billault C, Engelke M, Jimenez-Mateos EM, Wandosell F, Caceres A, Avila J: Participation of structural microtubule-associated proteins (MAPs) in the development of neuronal polarity. J Neurosci Res 2002;67:713–719.
27 Dehmelt L, Halpain S: Actin and microtubules in neurite initiation: are MAPs the missing link? J Neurobiol 2004;58:18–33.
28 Roger B, Al-Bassam J, Dehmelt L, Milligan RA, Halpain S: MAP2c, but not tau, binds and bundles F-actin via its microtubule binding domain. Curr Biol 2004;14:363–371.
29 Blobe GC, Stribling DS, Fabbro D, Stabel S, Hannun YA: Protein kinase C beta II specifically binds to and is activated by F-actin. J Biol Chem 1996;271:15823–15830.
30 Zhang W, Benson DL: Developmentally regulated changes in cellular compartmentation and synaptic distribution of actin in hippocampal neurons. J Neurosci Res 2002; 69:427–436.
31 Brose N: Synaptic cell adhesion proteins and synaptogenesis in the mammalian central nervous system. Naturwissenschaften 1999; 86:516–524.
32 Scholl FG, Scheiffele P: Making connections: cholinesterase-domain proteins in the CNS. Trends Neurosci 2003;26:618–624.
33 Dean C, Scholl FG, Choih J, DeMaria S, Berger J, Isacoff E, Scheiffele P: Neurexin mediates the assembly of presynaptic terminals. Nat Neurosci 2003;6:708–716.
34 Yu Q, Holloway HW, Flippen-Anderson JL, Hoffman B, Brossi A, Greig NH: Methyl analogues of the experimental Alzheimer drug phenserine: synthesis and structure/activity relationships for acetyl- and butyrylcholinesterase inhibitory action. J Med Chem 2001; 44:4062–4071.
35 Radic Z, Taylor P: Peripheral site ligands accelerate inhibition of acetylcholinesterase by neutral organophosphates. J Appl Toxicol 2001;21(suppl 1):S13–S14.
36 Hoffman RC, Jennings LL, Tsigelny I, Comoletti D, Flynn RE, Sudhof TC, Taylor P: Structural characterization of recombinant soluble rat neuroligin 1: mapping of secondary structure and glycosylation by mass spectrometry. Biochemistry 2004;43:1496–1506.
37 Friedman A, Kaufer D, Shemer J, Hendler I, Soreq H, Tur-Kaspa I: Pyridostigmine brain penetration under stress enhances neuronal excitability and induces early immediate transcriptional response. Nat Med 1996;2: 1382–1385.
38 Birikh KR, Sklan EH, Shoham S, Soreq H: Interaction of 'readthrough' acetylcholinesterase with RACK1 and PKCbeta II correlates with intensified fear-induced conflict behavior. Proc Natl Acad Sci USA 2003;100: 283–288.
39 Patterson RL, van Rossum DB, Barrow RK, Snyder SH: RACK1 binds to inositol 1,4,5-trisphosphate receptors and mediates Ca2+ release. Proc Natl Acad Sci USA 2004;101: 2328–2332.
40 Chang BY, Chiang M, Cartwright CA: The interaction of Src and RACK1 is enhanced by activation of protein kinase C and tyrosine phosphorylation of RACK1. J Biol Chem 2001;276:20346–20356.
41 Chang BY, Harte RA, Cartwright CA: RACK1: a novel substrate for the Src protein-tyrosine kinase. Oncogene 2002;21:7619–7629.
42 Selkoe DJ: Alzheimer's disease is a synaptic failure. Science 2002;298:789–791.
43 Crino PB, Eberwine J: Molecular characterization of the dendritic growth cone: regulated mRNA transport and local protein synthesis. Neuron 1996;17:1173–1187.
44 Aakalu G, Smith WB, Nguyen N, Jiang C, Schuman EM: Dynamic visualization of local protein synthesis in hippocampal neurons. Neuron 2001;30:489–502.
45 Steward O, Wallace CS, Lyford GL, Worley PF: Synaptic activation causes the mRNA for the IEG Arc to localize selectively near activated postsynaptic sites on dendrites. Neuron 1998;21:741–751.
46 Dori A, Cohen J, Silverman WF, Pollack Y, Soreq H: Functional manipulations of acetylcholinesterase splice variants highlight alternative splicing contributions to murine neocortical development. Cereb Cortex 2005;15:419–430.
47 Layer PG, Weikert T, Alber R: Cholinesterases regulate neurite growth of chick nerve cells in vitro by means of a non-enzymatic mechanism. Cell Tissue Res 1993;273:219–226.
48 Galyam N, Grisaru D, Grifman M, Melamed-Book N, Eckstein F, Seidman S, Eldor A, Soreq H: Complex host cell responses to antisense suppression of ACHE gene expression. Antisense Nucl Acid Drug Dev 2001;11:51–57.
49 Petralia RS, Wang YX, Wenthold RJ: The NMDA receptor subunits NR2A and NR2B show histological and ultrastructural localization patterns similar to those of NR1. J Neurosci 1994;14:6102–6120.
50 Tingley WG, Ehlers MD, Kameyama K, Doherty C, Ptak JB, Riley CT, Huganir RL: Characterization of protein kinase A and protein kinase C phosphorylation of the N-methyl-D-aspartate receptor NR1 subunit using phosphorylation site-specific antibodies. J Biol Chem 1997;272:5157–5166.
51 Dunah AW, Standaert DG: Dopamine D1 receptor-dependent trafficking of striatal NMDA glutamate receptors to the postsynaptic membrane. J Neurosci 2001;21:5546–5558.
52 Grant SG, O'Dell TJ, Karl KA, Stein PL, Soriano P, Kandel ER: Impaired long-term potentiation, spatial learning, and hippocampal development in fyn mutant mice. Science 1992;258:1903–1910.
53 Stebbings H: Cytoskeleton-dependent transport and localization of mRNA. Int Rev Cytol 2001;211:1–31.
54 Chen J, Kanai Y, Cowan NJ, Hirokawa N: Projection domains of MAP2 and tau determine spacings between microtubules in dendrites and axons. Nature 1992;360:674–677.
55 Felgner H, Frank R, Biernat J, Mandelkow EM, Mandelkow E, Ludin B, Matus A, Schliwa M: Domains of neuronal microtubule-associated proteins and flexural rigidity of microtubules. J Cell Biol 1997;138:1067–1075.
56 Ozer RS, Halpain S: Phosphorylation-dependent localization of microtubule-associated protein MAP2c to the actin cytoskeleton. Mol Biol Cell 2000;11:3573–3587.
57 Meshorer E, Biton IE, Ben-Shaul Y, Ben-Ari S, Assaf Y, Soreq H, Cohen Y: Chronic cholinergic imbalances promote brain diffusion and transport abnormalities. FASEB J 2005; 19:910–922.
58 Darreh-Shori T, Hellstrom-Lindahl E, Flores-Flores C, Guan ZZ, Soreq H, Nordberg A: Long-lasting acetylcholinesterase splice variations in anticholinesterase-treated Alzheimer's disease patients. J Neurochem 2004;88:1102–1113.
59 Markram H, Segal M: Long-lasting facilitation of excitatory postsynaptic potentials in the rat hippocampus by acetylcholine. J Physiol 1990;427:381–393.
60 Segal M, Auerbach JM: Muscarinic receptors involved in hippocampal plasticity. Life Sci 1997;60:1085–1091.
61 Markram H, Segal M: The inositol 1,4,5-trisphosphate pathway mediates cholinergic potentiation of rat hippocampal neuronal responses to NMDA. J Physiol 1992;447: 513–533.
62 Segal M: Acetylcholine enhances NMDA-evoked calcium rise in hippocampal neurons. Brain Res 1992;587:83–87.